Electronic Supplementary Information for "Mechanical properties of tantalum carbide from high-pressure/high-temperature synthesis and first-principles calculations"

Weiguo Sun,[1,2,3,*] Xiaoyu Kuang,[1,*] Hao Liang,[1] Xinxin Xia,[1]
Zhengang Zhang,[4] Cheng Lu,[1,2,†] and Andreas Hermann[3,‡]

[1] *Institute of Atomic and Molecular Physics, Sichuan University, Chengdu 610065, China*

[2] *School of Mathematics and Physics, China University of Geosciences (Wuhan), Wuhan 430074, China*

[3] *Centre for Science at Extreme Conditions and SUPA, School of Physics and Astronomy, The University of Edinburgh, Edinburgh EH9 3FD, United Kingdom*

[4] *Mechanical Engineering Department of Qinghai University, Xining, 810016, China*

The HPHT experiments are carried out with a DS 6-14 MN cubic press. The samples are slowly compressed to 5.5 GPa, followed by heating to 1400 °C with a heating rate of 150 °C/min. Subsequently, the sample is quenched to room temperature at a cooling rate of 150 °C/min, and then decompressed to ambient pressure. More experimental detailed procedures can be found elsewhere [1–3]. The sintered TaC sample is analyzed using our in-house X-ray diffractometer (DX-2500, Dandong, China & model X'pert MPD, Philips, Holland) at 0.01°/s for 2θ = 10° - 100° to inspect the crystal structure and phase identification. The fracture surfaces are studied by Scanning Electron Microscopy (SEM; JSM-6490, JEOL, Akishima, Japan) to detect the microstructure of the samples [2], see Fi. S1 for representative micrographs. Vickers hardness (H_v) tests are conducted on the ends-polished samples by means of Vickers single crystalline diamond indenter (FV-700, Future-Tech Corp. Japan). H_v is determined as [4]: $H_v = 1854.4 \times F/L^2$, F (in N) is the applied load, and L (in μm) is the arithmetic mean of the two diagonals of the Vickers indentation that can be measured by SEM. In our experiment, eight hardness data points are obtained for each sintered sample at different loading force and holding time for 15 s [2]. One sample is measured for hardness at different loading forces ($\sim$ 30 N as the highest loading) to confirm that the hardness under 19.6 N is close to the asymptotic value.

For variable structural candidates, we have used the CALYPSO [5–7] package to search the

*Contributed equally to this work
†Electronic address: lucheng@calypso.cn
‡Electronic address: a.hermann@ed.ac.uk

ground state crystal structure of the TaC. The validity and efficiency of CALYPSO method in structure prediction has been demonstrated by the accuracies in large variety of systems [8–10]. The structure searches have successfully identified the truly ground state of TaC is cubic structure, with $Fm\bar{3}m$ symmetry, which is confirmed by our follow up experiment. We have performed the calculations of ideal indentation strength using the newly developed Vickers indenter method [11–13] in conjunction with Vienna Ab Initio Simulation Package (VASP) [14]. The electron-ion interaction is described by projector augmented wave (PAW) potentials [15, 16] in plane wave basis set. The generalized gradient approximation (GGA) Perdew-Burke-Ernzerhof (PBE) [17] functional is employed to model exchange-correlation effects in the electron-electron interaction. The frozen core all-electron PAW method is adopted with $6s^2 5d^3$ and $2s^2 2p^2$ states treated as valence electrons for Ta and C, respectively. We have set the plane wave cutoff energy to 800 eV in all structural relaxations and electronic calculations, and $15\times15\times15$ Monkhorst-Pack [18] grids for the reciprocal space sampling are chosen during atomic relaxations, see Fig. S3 for convergence properties. All total energies are converged to better than 10^{-6} eV in the SCF run, and residual stresses and forces after full atomic relaxations are less than 0.1 GPa and 0.001 eV/Å, respectively. Elastic constants were determined by performing six finite distortions of the lattice and deriving the elastic constants from the strain-stress relationship implemented in VASP [19].

To uncover the detailed relationship between hardness and crystal structure, the electronic structure of TaC has been researched by detailed first principles calculations. The electron localization function (ELF) [20] analysis of TaC is displayed in Fig. S4(a) and Fig. S5 for both equilibrium and critical strain, and indicates local electron paring surrounding the C atoms in both cases. The ELF suggests electron transfer from Ta atoms to C atoms, which is consistent with our Bader charge analysis [21]: the charge transferred from Ta to C is about 1.684 electrons (1.605 electrons at V_1). As shown in Fig. S4(b), TaC is dynamically stable, as evidenced by our calculated phonon dispersion curves that have no imaginary phonon modes. Fig. S4(c, d) show the calculated valence electron total and projected density of states (DOS) and the electronic band structure. The occupied states (about -8 $\sim$ 4.00 eV) are mainly contributed by d states from tantalum and p states from carbon. Strong p-d hybridization emerges around -5 eV below the Fermi energy. Several energy bands cross the Fermi level to indicate the metallic character of TaC, which is dominated by Ta d states.

Moreover, we have analysed the Crystal Orbital Hamilton Populations (COHP) [22–24] to examine the evolution of the bonding properties along the strain field, for specific Ta-C bonds (see Fig. S5(a)). In Fig. S5(b), the COHP provide an estimate of the strength for the marked

Ta-C bonds both before and after structural failure. For the equilibrium structure V_0 ($\varepsilon = 0$), the Ta_2 and Ta_3 atoms show the same bonding strength when bonding to the central C atom because of ideal face-centered cubic symmetry. With the increasing Vickers strain, the Ta_2-C and Ta_3-C bonds in the [001] plane are shortened to 2.21 Å, while bonds along the [001] axis are stretched to 2.30-2.31 Å at $\varepsilon = 0.260$, which is agreement with the gradual increase of -ICOHP values (see Fig. 3 in the main manuscript). At the critical strain, shown as V_1 in Fig. S6(b), the COHP curves are largely unchanged from V_0. As the strain increases to 0.265, the three-dimensional network has been broken and reconstructed, with drastic consequences for the COHP (shown as the V_2 in Fig. S6(b)). For the Ta_1-C bond, which changes from disconnected bonding status at V_0 and V_1 to strong directional Ta-C bonding at V_2, the -ICOHP increases correspondingly from 0 to 2.84. Meanwhile, the Ta_3-C bond has been broken through sliding [010] planes of atoms along the $[\bar{1}01]$ direction, resulting in a sharp decline form 3.60 to 0.02 in -ICOHP. When the strain continues to increase, the new structure based on V_2 connectivity relaxes further, and the Ta_1-C bond recovers to the equilibrium value (see Fig. 3(d) in the main manuscript), which correspends to our prior structural analysis.

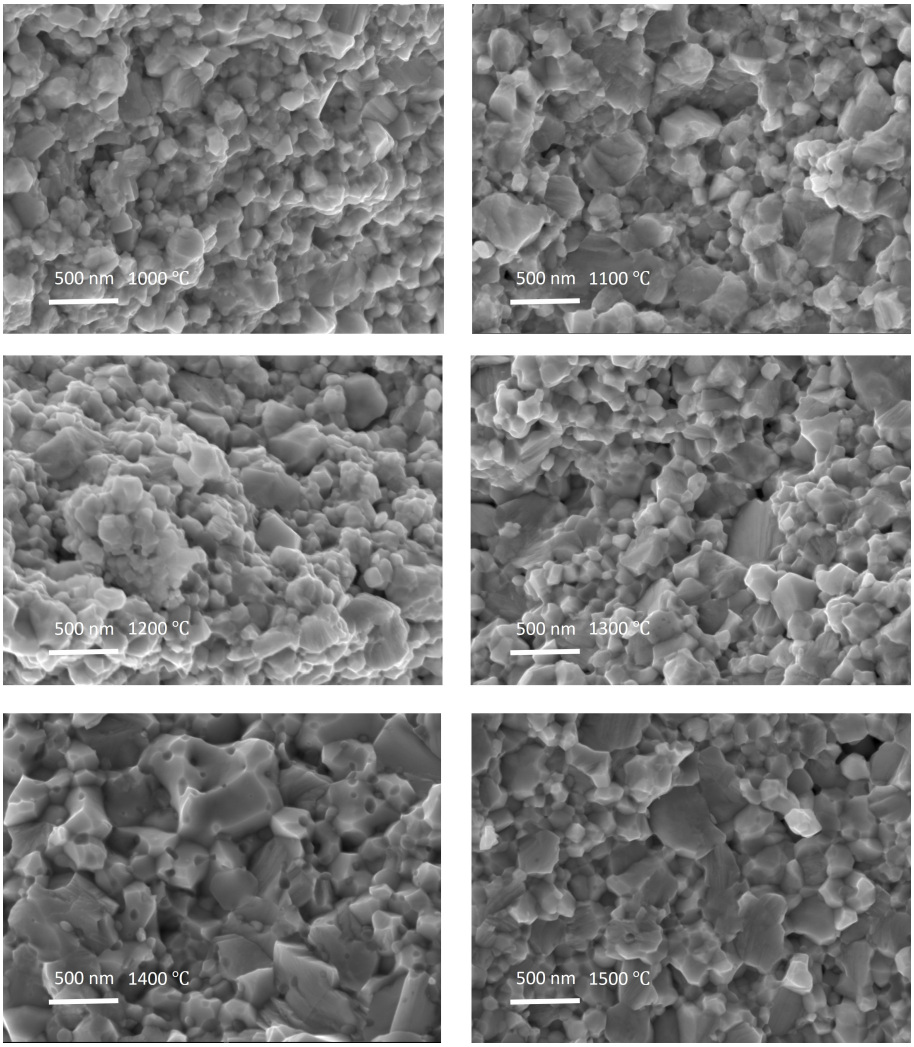

FIG. S1: SEM micrographs of TaC samples synthesized at 5.5 GPa and different temperatures. From top left to bottom right: T=1000 – 1500 °C.

TABLE S1: The calculated peak strains and stresses (GPa) for TaC in various directions under uniaxial (tensile) deformation.

Uniaxial	Tensile[001]		Tensile[110]		Tensile[111]	
	ε_{max}	σ_{max}	ε_{max}	σ_{max}	ε_{max}	σ_{max}
TaC	0.140	42.3	0.290	60.0	0.205	70.5

[1] G. Liu, *et al*. Appl. Phys. Lett. 2015, **106**, 121901.

[2] H. Liang, *et al*, Mater. Sci. Eng., A, 2018 **711**, 389.

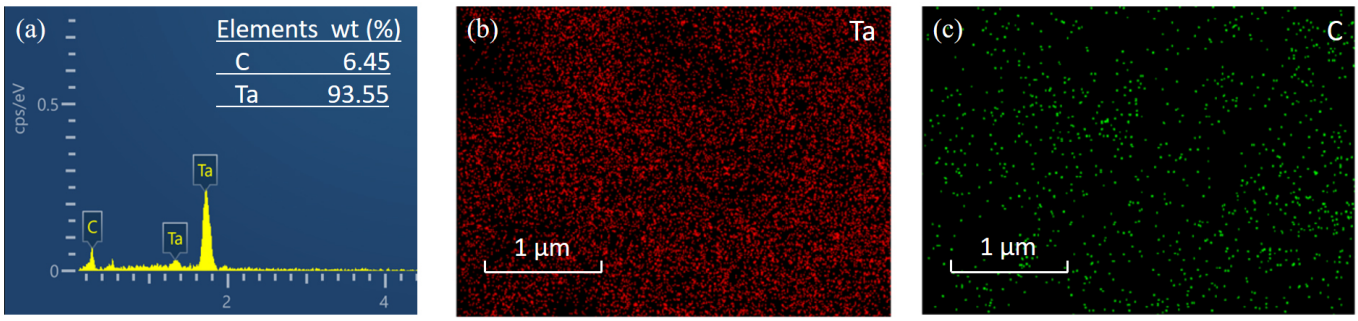

FIG. S2: (a) Element content from energy-dispersive X-ray spectroscopy (EDS) point scans, (b, c) the corresponding EDS compositional maps of TaC samples.

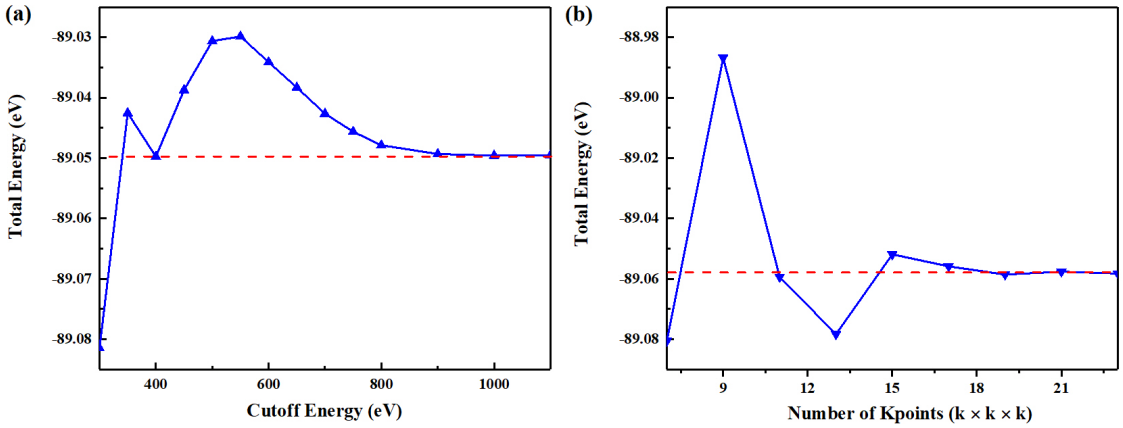

FIG. S3: Convergence of total energy per conventional unit cell of TaC as (a) function of plane wave cutoff and (b) size of the Monkhorst-Pack k-point grid.

[3] H. Liang, *et al*, Ceram. Int., 2019 **45**, 7885.

[4] M. D. Drory, J. W. Ager, T. Suski, I. Grzegory, and S. Porowski, Appl. Phys. Lett., 1996 **69**, 4044.

[5] Y. Wang, J. Lv, L. Zhu, and Y. Ma, Comput. Phys. Commun., 2012 **183**, 2063.

[6] Y. Wang, J. Lv, L. Zhu, and Y. Ma, Phys. Rev. B, 2010 **82**, 094116.

[7] B. Gao, P. Gao, S. Lu, J. Lv, Y. Wang, and Y. Ma, Sci. Bull., 2019 **64**, 301.

[8] C. Lu, M. Miao, and Y. Ma, J. Am. Chem. Soc., 2013 **135**, 14167-14171.

[9] C. Lu, Q. Li, Y. Ma, and C. Chen, Phys. Rev. Lett., 2017 **119**, 115503.

[10] J. Lv, Y. Wang, L. Zhu, and Y. Ma, Phys. Rev. Lett., 2011 **106**, 015503.

[11] C. Zang, H. Sun, J. S. Tse, and C. Chen, Phys. Rev. B, 2012 **86**, 014108.

[12] Z. Pan, H. Sun, and C. Chen, Phys. Rev. Lett., 2007 **98**, 135505.

[13] Z. Pan, H. Sun, Y. Zhang, and C. Chen, Phys. Rev. Lett., 2009 **102**, 055503.

[14] G. Kresse and D. Joubert, Phys. Rev. B, 1999 **59**, 1758.

[15] G. Kresse and J. Furthmüller, Phys. Rev. B, 1996 **54**, 11169.

[16] G. Kresse and J. Furthmüller, Comput. Mater. Sci., 1996 **6**, 15.

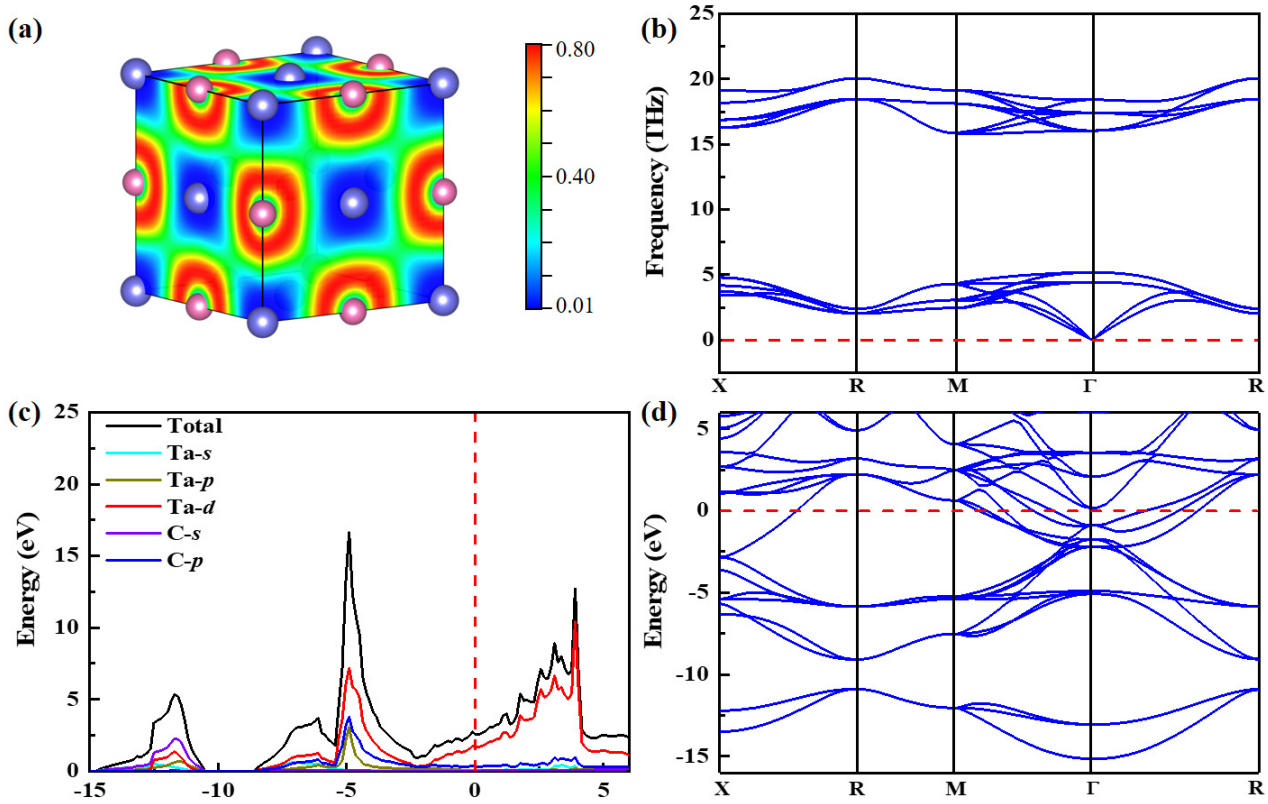

FIG. S4: (a) Electron localization function (ELF) analysis of TaC crystal (blue - Ta; pink - C), (b) phonon dispersion curve for TaC, (c) total and partial electronic density of states, (d) electronic band structure of TaC system.

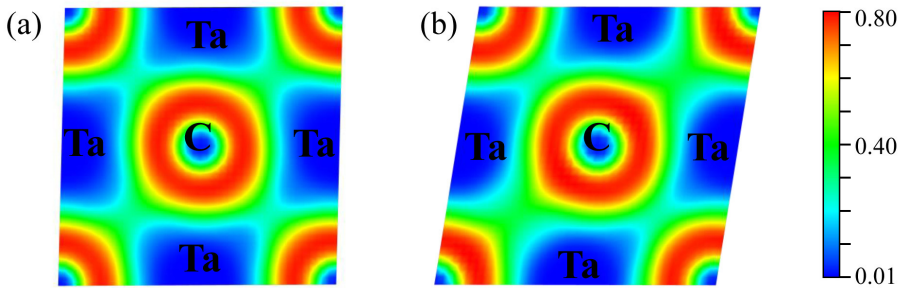

FIG. S5: (a, b) Represent the electron localization function (ELF) iso-surface of TaC crystal under the maximum pure shear and Vickers shear in (001) plane when strain $\varepsilon = 0.370$ and 0.215, respectively.

[17] J. P. Perdew, K. Burke, and M. Ernzerhof, Phys. Rev. Lett., 1996 **77**, 3865.

[18] H. J. Monkhorst, and J. D. Pack, Phys. Rev. B, 1976 **13**, 5188.

[19] Y. Le Page, P. Saxe, Phys. Rev. B, 2002 **65**, 104104.

[20] A. D. Becke and K. E. Edgecombe, J. Chem. Phys., 1990 **92**, 5397-5403.

[21] R. F. W. Bader, Acc. Chem. Res., 1985 **18**, 9.

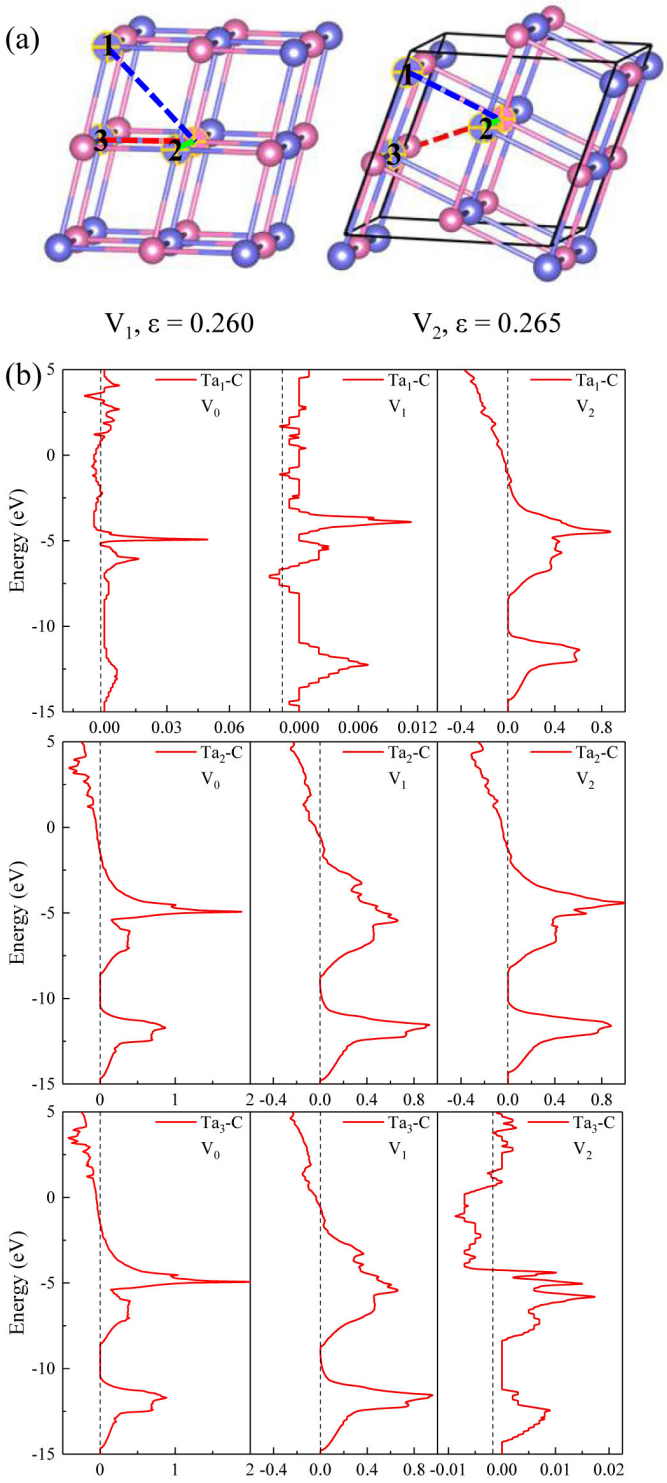

FIG. S6: (a) Structural snapshots show TaC at key points before and after the structural change induced by Vickers strain along the $(1\bar{1}0)[001]$ direction and point out specific Ta-C bonds. (b) Crystal orbital Hamilton population (COHP) curves for different Vickers shear strains along the $(1\bar{1}0)[001]$ direction, for the bonds shown in (a).

[22] R. Dronskowski and P. E. Blochl, J. Phys. Chem., 1993 **97**, 8617.

[23] V. L. Deringer, A. L. Tchougreeff, and R. Dronskowski, J. Phys. Chem. A, 2011 **115**, 5461.

[24] S. Maintz, V. L. Deringer, A. L. Tchougreeff, and R. Dronskowski, J. Comput. Chem. 2016 **37**, 1030.